Anion efflux mediates transduction in hair cells of zebrafish lateral line

Elias T. Lunsford[1]*, Yuriy V. Bobkov[1]*, Brandon C. Ray[1], James C. Liao[1], James A. Strother[1]

[1]Department of Biology, The Whitney Laboratory for Marine Bioscience, University of Florida; Saint Augustine, FL USA 32080

Corresponding author. Email: james.strother@whitney.ufl.edu (J.A. Strother) and jliao@whitney.ufl.edu (J.C. Liao)

*These authors contributed equally to this work

Abstract:

Hair cells are the principal sensory receptors of the vertebrate auditory system, and transduce sounds with mechanically-gated ion channels that permit cations to flow from the surrounding endolymph into the cells. The lateral line of zebrafish has served as a key model system for understanding hair cell physiology and development, and it has often been speculated that these hair cells employ a similar transduction mechanism. In this study, we demonstrate that the hair cells are exposed to an unregulated external environment with cation concentrations that are too low to support transduction. Instead, our results indicate that hair cell excitation is mediated by a fundamentally different mechanism involving the outward flow of anions.

Main:

Vertebrate hair cells are ciliated mechanoreceptive sensory cells responsible for the exquisite sensitivity of the auditory and vestibular systems. In the auditory system, these cells are immersed in endolymph with a relatively high K^+ concentration and positive potential, which establishes a strong electrochemical gradient favoring K^+ influx into the cells[1–3]. Sound propagating through the cochlea generates shearing forces on the apical stereocilia bundle of hair cells. Deflection of the stereocilia opens mechanically-coupled cation channels (i.e., TMC1/2[4–6]),

which permits K^+ influx into the hair cells (mechanoelectrical transduction [MET] current) and drives membrane depolarization[7,8]. The high K^+ concentration of the endolymph is key to this pathway, and is produced by active secretion of K^+ into the endolymph by strial marginal cells via a process that includes K^+ channels and Na^+/K^+ ATPase[9–11].

The hair cells of the inner ear are thought to have evolved from anatomically similar cells found in the lateral line of fishes and amphibians (reviewed by[12]). The lateral line system detects the movement of water around the body and is critical for survival, as it mediates behaviors such as predator avoidance, prey capture, and navigation[13–16]. Unlike the hair cells of the inner ear, the lateral line hair cells lie on the surface of the body and are surrounded by the external environment rather than a K^+-rich endolymph. Work in amphibians in the 1970s indicated that the gelatinous cupula that encapsulates the lateral line hair cells maintains an ionic microenvironment comparable to the inner ear endolymph, which establishes the ionic gradient necessary for cation influx mediated mechanotransduction[17,18].

Although freshwater zebrafish are a powerful model system for understanding hair cell physiology[19–21], this foundational hypothesis has remained largely untested. Here, we show that the ionic microenvironment in the cupula of the superficial neuromasts of zebrafish larvae is indistinguishable from the surrounding freshwater. Electrochemical calculations indicate that the freshwater inhabited by zebrafish does not provide ionic gradients sufficient to support the putative cation-mediated mechanotransduction mechanism. Instead, our results suggest a novel process driven by anion efflux. For cells in contact with ion-poor extracellular saline, typical negative resting membrane potentials and intracellular Cl^- concentrations are sufficient to generate anion efflux capable of inducing robust membrane depolarization. Although studies of sensory physiology often focus on cation mediated transduction process, anion efflux has been observed to contribute to signal amplification in vertebrate chemosensory receptors, which often

directly interface with an unregulated external environment[22–26]. It has also been argued that anion efflux may confer favorable properties, including reduced sensitivity to large variations in extracellular ionic composition[27,28].

The cupula does not provide a cation-rich microenvironment for lateral line hair cells

We first examined if the cupula of the superficial neuromasts contained an elevated K^+ concentration capable of supporting mechanotransduction. Animals were bathed in a freshwater media (E3 saline) with a K^+ selective fluorescent indicator (IPG-4). Using confocal microscopy, we found that fluorescence in the cupula was nearly indistinguishable from that of the surrounding water, suggesting that the cupula does not maintain elevated K^+ concentrations (Fig. 1B). To quantify the K^+ concentration within the cupula, the indicator was saturated by adding K^+ to the surrounding media, and the recorded fluorescence values were fit to a model that incorporates both the binding affinity of the indicator and potential differences in indicator concentration between the cupula and media. Consistent with our qualitative observations, the calculated K^+ concentration of the cupula was not significantly different from the surrounding media ($p = 0.49$, $N=14$; Fig. 1C). Analogous experiments were then performed examining each of the major cations present in freshwater saline and again no significant differences were found between the cupula and the surrounding water (Na^+: $p = 0.23$, $N=9$; Ca^{2+}: $p = 0.54$, $N = 9$; H^+: $p = 0.38$, $N=9$; Fig. 1D). We also examined the Cl^- concentration within the cupula, since it is the likely counterion for any cation, and found that it was also not significantly different from the freshwater media ($p=0.43$, $N=6$, Fig. 1D). These results indicate that the cupula does not support an ionic microenvironment, and the apical surfaces of the lateral line hair cells are directly exposed to an ion-poor freshwater saline that is markedly different from the endolymph of the inner ear[2,3,29–31].

To systematically explore the consequences of the hair cells being exposed to an ion-poor environment, we calculated the membrane reversal potential for a MET channel in different extracellular solutions, assuming relative permeabilities similar to other hair cells. We found that in freshwater media (E3 saline), MET conductance would be expected to produce K^+ efflux and hyperpolarization rather than depolarization, which strongly suggests that K^+ current is not the primary driver of transduction (Fig. 1E). MET conductance is only predicted to induce membrane depolarization sufficient to open the voltage-gated Ca^{2+} channels on the basolateral membrane ($Ca_V1.3$[32]) in water with cation concentrations much greater than those in the natural habitat of zebrafish (Fig. 1E[29–31]). Although the chemical gradient favors Ca^{2+} influx into the hair cell, this influx is unable to overcome the hyperpolarizing effect generated by K^+ efflux given the estimated relative permeabilities of the MET channels. Ca^{2+} currents would therefore only be sufficiently depolarizing if the MET channels displayed Ca^{2+} selectivity far in excess of that reported in other systems[4]. We next calculated the reversal potential for a hypothetical Cl^- channel and found that Cl^- conductance would be expected to readily drive Cl^- efflux from the hair cells and membrane depolarization in a wide range of external environments (Fig. 1E). In total, these results argue against K^+ influx as a mechanism for lateral line hair cell depolarization and suggest that Ca^{2+} influx or Cl^- efflux may have more central roles.

The lack of an ionic microenvironment in the cupula would profoundly affect the mechanotransduction mechanisms available to hair cells. We next conducted a series of experiments and simulations further exploring whether the physical properties of the cupula could support such a microenvironment. We first examined the diffusion of charged molecules within the cupula by rapidly introducing a negatively charged small molecule fluorophore (6-carboxyfluorescein; 6-CF) around the cupula and imaging its diffusion from the media into the cupula (Fig. 1F). There were no significant differences between the rate at which fluorescence

increased in the cupula and the surrounding water, suggesting that charged molecules rapidly penetrate the cupula (relative time constant = 0.88 ± 0.06 [mean ± S.E.M.], p = 0.076, N=9, Fig. 1G). Computational simulations confirmed this experimental setup had sufficient resolution to detect meaningful differences in the diffusive properties of the cupular matrix (Extended Data Fig. 1). This finding is also consistent with empirical studies of the ultrastructure of lateral line cupulae, which identified no membrane or other dense surface structure[33,34].

We next evaluated the ion currents that would be necessary to sustain a K^+ reservoir in the cupula using computational simulations. Since this configuration violates the assumptions of a typical neuron electrical equivalent circuit[35], we simulated these dynamics by directly solving the full three-dimensional Nernst-Planck equations using the finite element method (Fig. 1H). Based on the above diffusion experiments, we estimated the diffusion coefficients for ions moving through the cupular matrix to be similar to water and assumed a constant rate of K^+ secretion into the matrix at the base of the neuromast. We found that a K^+ current 56 nA would be needed to produce the K^+ concentration of 10.2 mM required for depolarizing MET conductance (Fig. 1E&I). Although the ionoregulatory currents of the neuromast have not been quantified, these K^+ current values are several orders of magnitude greater than the resting MET current of hair cells[36,37]. These results indicate that recently described skin-derived ionocytes are unlikely to maintain a K^+ microenvironment at the apical surface of the hair cells, but may instead support regulation of the extracellular environment at the basolateral surfaces[38].

Cumulatively, these experiments indicate that the cupula does not maintain a cation rich microenvironment sufficient to support hair cell depolarization, challenging a long-standing assumption that hair cell transduction is cation driven in the lateral line system of zebrafish and other freshwater fishes.

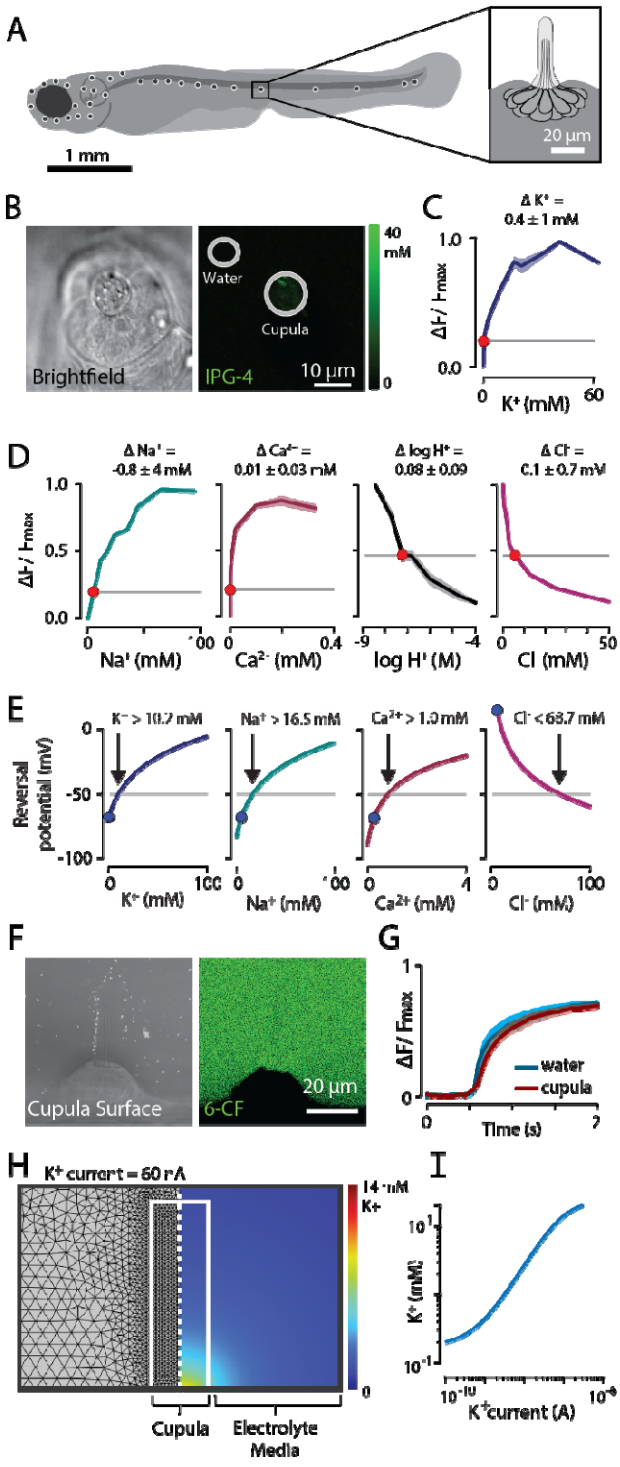

Fig. 1. The ionic microenvironment of the cupula resembles freshwater and cannot support cation influx mediated depolarization. (A) Superficial neuromasts of the lateral line system in larval zebrafish. **(B)** *In vivo* visualization of K^+ in the vicinity of a neuromast using the fluorescent probe IPG-4 (left: brightfield; right: IPG-4). **(C)** Fluorescence of K^+ probe in

127 solutions with varying K^+ concentrations (blue curve), fluorescence expected for an environment
128 matching surrounding freshwater media (E3 saline; horizontal grey line), and measured
129 fluorescence within the cupula (red dot, error bars are ± SEM). Using these values, the difference
130 between the K^+ concentration in the cupula and the surrounding media was calculated (ΔK^+,
131 mean ± SEM). **(D)** Results from experiments similar to (C) except examining Na^+ (probe: ING-
132 2), Ca^{2+} (probe: Fluo-5N), H^+ (probe: BCECF), and Cl^- (probe: MQAE). In all cases, ion
133 concentrations within the cupula matched those of the surrounding media. **(E)** Predicted reversal
134 potentials for MET channels as a function of cupula cation concentration. The estimated opening
135 potential of voltage-gated Ca^{2+} channels at the basal membrane is indicated (-50 mV, horizontal
136 line). The cation concentration necessary to reach this potential (black arrow) and the
137 concentration in freshwater media (blue dot) are also indicated. The predicted reversal potential
138 for a hypothetical chloride channel is also shown (right). **(F)** Images showing penetration of a
139 charged fluorophore (6-carboxyfluorescein, 6-CF) into neuromast cupula (left: cupula surface
140 visualized with microspheres, right: 6-CF). **(G)** From the same experiments as (F), time series
141 showing rapid increase in fluorescence in both media around the cupula and within the cupula
142 after introduction of the charged fluorophore. **(H)** Simulation of a hypothetical K^+
143 microenvironment, produced by solving 3D Nernst-Plank equations (left: mesh, right: K^+
144 distribution for K^+ current = 60nA). **(I)** K^+ concentration at apical surface of hair cells as a
145 function of K^+ secretion current.
146

147 ***Lateral line function only requires micromolar extracellular calcium***

148 What other mechanisms could mediate hair cell depolarization? We next tested the hypothesis
149 that Ca^{2+} could contribute to hair cell depolarization, given its reversal potential and assuming
150 MET channels with unusually high Ca^{2+} selectivity. Hair cells expressing the fluorescent calcium
151 indicator GCaMP6s were imaged while mechanically deflecting the cupula with a piezoelectric
152 transducer (Fig. 2A). Changes in fluorescence near the basal surface of the hair cells were
153 observed, which have been attributed to Ca^{2+} influx through voltage-gated channels on the basal
154 membrane[21]. Hair cells produced robust responses to this stimulus in freshwater media (E3
155 saline, 330 µM Ca^{2+}; $p < 0.001$, $df = 27$; Fig. 2A). Interestingly, we found that hair cells
156 continue to respond in media with substantially reduced Ca^{2+} concentrations (20 µM Ca^{2+}; $p =$
157 0.04, $df = 3$; Fig 2A) and that these responses were indistinguishable from those observed in
158 freshwater media ($p = 0.13$, $df = 3$). The insensitivity of hair cell responses to available Ca^{2+}
159 suggests that Ca^{2+} is not the principal carrier of the MET current. However, responses in 0 µM
160 Ca^{2+} media were significantly reduced compared to those in freshwater media ($p = 0.02$, $df = 9$;
161 Fig 2A). This indicates that environmental Ca^{2+} modulates MET currents in naturalistic
162 freshwater media, consistent with observations of Ca^{2+} effects on hair cell mechanotransduction
163 in zebrafish and other species[8,39–43].
164

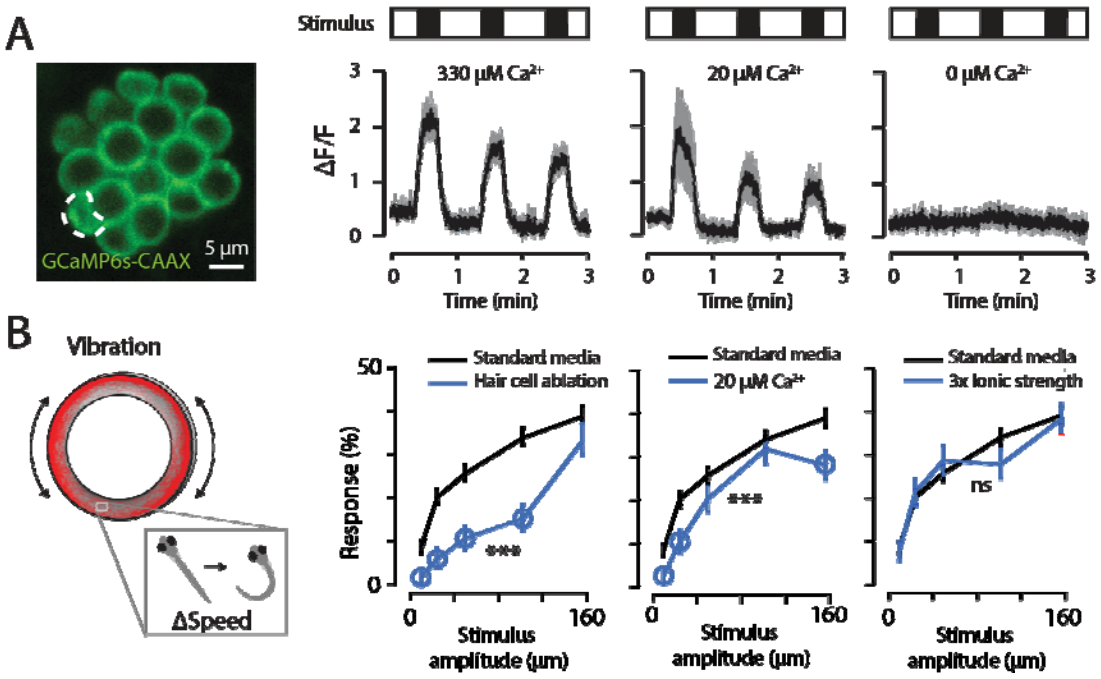

Fig. 2. Only micromolar extracellular calcium is required for lateral line function.

(A) Response of hair cells to a mechanical stimulus, recorded by imaging genetically expressed fluorescent calcium indicator GCaMP6s-CAAX at the basal membrane (left: typical image, region of interest indicated; right: responses in 330 µM, 20 µM, and 0 µM Ca^{2+}, mean ± SEM). Hair cell responses in micromolar Ca^{2+} media are comparable to those in freshwater media (E3 saline), while responses are abolished in calcium-free media. **(B)** Behavioral response of zebrafish larvae to a mechanical stimulus under varying conditions, recorded with a novel behavioral assay that employs an oscillatory Couette cell to produce a pure-shear flow stimulus (left: schematic of behavioral setup with typical trajectory in red; left: probability of response following neomycin-induced hair cell ablation, in 20 µM Ca^{2+} media, and in 3x ionic strength media). Asterisks indicate statistically significant differences integrated across stimulus intensities (*p<0.05, **p<0.01, ***p<0.001), open circles represent significant pairwise comparisons (p<0.05), and results are shown as mean ± SEM.

To verify that these cellular-scale differences are reproduced at the organismal level, we next examined the effects of low Ca^{2+} environments on the behavior of freely swimming larvae. A number of behavioral assays have been successfully employed for assessing lateral line function in zebrafish larvae, including assays measuring C-start escapes in response to impulsive stimuli and assays measuring rheotactic responses[13–15]. However, the contribution of multiple sensory modalities (e.g. vestibular, acoustic, visual) to behavioral responses often presents a challenge when developing such assays. Since the superficial lateral line is principally sensitive to shear at the body surface[44], we designed a novel behavioral assay that uses an oscillatory Couette cell to produce a shearing flow without accompanying pressure waves (Extended Data Fig. 2). The position and swimming speed of animals were continuously monitored, and stimuli of varying intensities were presented at random intervals. Each stimulus that produced a significant change in swimming speed (outside 95% confidence interval) was recorded and then the net response probability was calculated as a function of stimulus intensity. In order to reduce both habituation and activation of collateral sensory modalities, we intentionally examined small stimulus intensities that produced modest changes in behavior with relatively low response probabilities rather than escape responses with high probability.

To verify the efficacy of this assay, we confirmed that animals responded in an intensity-dependent manner and that neomycin-induced hair cell ablation dramatically decreased this response (Fig. 2B). Next, we examined how low environmental Ca^{2+} affects lateral line sensitivity and found that animals displayed reduced but robust responses even with Ca^{2+} decreased by >15x (21% decrease with 50 μm stimulus, omnibus $p < 0.001$, N = 30 exp/94 ctrl). These results are consistent with our imaging data and data from other species[39,45]. Using this same assay, we then examined how lateral line sensitivity is altered by increases in the ionic strength of the freshwater environment. The responses of animals in media with a 3x increase in

ionic strength were not significantly different from those in freshwater media (E3 saline, omnibus $p > 0.05$, N=30 exp/94 ctrl). Media with higher ion concentrations were also explored, and significant decreases in sensitivity were detected, but such ion concentrations far exceed the values observed in the natural habitat of zebrafish and these effects may result from osmotic stress rather than a specific interaction with the lateral line (Extended Data Fig. 3). In total, these findings strongly suggest that extracellular Ca^{2+} modulates the mechanotransduction process but is not the primary ion current driving hair cell depolarization.

Calcium-activated anion efflux contributes to hair cell depolarization

Since the electrochemical gradient between hair cells and freshwater strongly favors anion efflux, we next examined whether this efflux could be contributing to mechanotransduction. We began by leveraging available transcriptome data to generate testable hypotheses. We analyzed published transcriptome scRNA-seq data collected from zebrafish lateral line neuromasts [46] for cells that expressed a hair cell marker (tmc2b), filtered transcripts for genes associated with ion channel activity, and then reviewed the resulting list for genes with anion efflux activity. This analysis indicated that the lateral line hair cells may express the calcium-activated anion channel Anoctamin-2b (ANO2b), also known as TMEM16b (Fig. 3A).

To verify this expression, *ano2b* transcripts were labeled using HCR RNA-FISH. We observed *ano2b* labeling in lateral line hair cells, olfactory epithelium, and the dorsal habenula (Fig. 3B & S4). The expression of anoctamin in the olfactory epithelium is consistent with similar findings in mammalian olfactory epithelium[47], and *ano2b* expression in the dorsal habenula of zebrafish has been previously reported[48].

We next examined if calcium-activated chloride channels are capable of inducing depolarization of the lateral line hair cells. Using zebrafish larvae that express a fluorescent

calcium indicator in hair cells (*myo6b:GCaMP6s-CAAX*[21]), we recorded hair cell responses to the Anoctamin2 agonist Eact[49]. This agonist induced immediate and robust increases in intracellular calcium at the basolateral membrane ($p < 0.001$, $df = 58$), which were reversible upon washout (Fig. 3C). These responses are consistent with the hypothesis that calcium-activated anion channels contribute to mechanotransduction in the lateral line hair cells.

We then sought to determine if these effects were reflected in the responses of an intact, behaving animal. When we examined the behavioral response of animals that had been treated with the calcium-activated chloride channel blocker niflumic acid (NFA)[50], we found that they exhibited a marked decrease in behavioral responses relative to untreated animals (48% decrease with 50 µm stimulus, omnibus $p < 0.001$, N=30 exp/94 ctrl, Fig. 3D). We also examined the sensitivity of animals in media in which Cl^- concentrations were varied to manipulate the strength of the electrochemical gradient supporting anion efflux. We found that increasing this electrochemical gradient by reducing extracellular Cl^- (0.8 mM) produced a small increase in the response to stimuli relative to freshwater media (5.2 mM), although this effect was not significant (omnibus $p > 0.05$, N=30 exp/94 ctrl, Fig. 3E). Conversely, we found that decreasing this gradient by increasing extracellular Cl^- (16 mM) reduced the response (27% decrease with 50 µm stimulus, omnibus $p < 0.01$, N=30 exp/94 ctrl, Fig. 3E) relative to freshwater media. This suppression, but not termination, of lateral line sensitivity is consistent with the reversal potential still favoring anion efflux at this extracellular Cl^- concentration (Fig. 1E). Higher Cl^- concentrations were examined and similar results were observed (Extended Data Fig. 3), although such salines impose a stronger osmostic stress that may complicate interpretation. Cumulatively, these results provide further support for the role of anion efflux in lateral line mechanotransduction.

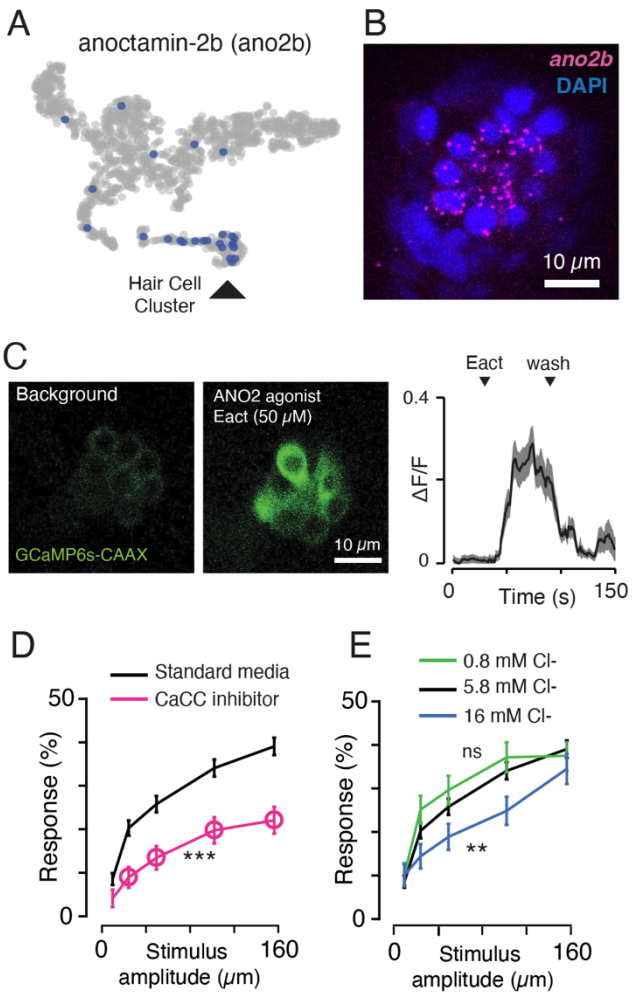

Fig. 3. Calcium-activated chloride channels are expressed in lateral line hair cells, sufficient to activate hair cells, and necessary for functional responses at the organismal level.

A) Visualization of single cell transcriptome data for lateral line neuromast showing expression of anoctamin-2b (*ano2b*) in the hair cell cluster (t-SNE plot, data from[46]). (**B**) *In situ* hybridization image showing *ano2b* expression in a lateral line neuromast (punctate pattern consistent with single-molecule RNA-FISH). (**C**) Response of hair cells to the Ano2 agonist Eact, recorded at the basal membrane using a genetically expressed fluorescent calcium indicator (left and middle: typical images, right: measured ΔF/F for introduction and washout, mean ± SEM.). (**D**) Effect of the calcium-activated chloride channel (CaCC) inhibitor NFA on the behavioral response of zebrafish larvae to a mechanical stimulus. Asterisks indicate statistically

263 significant differences integrated across stimulus intensities (*p<0.05, **p<0.01, ***p<0.001),
264 open circles represent significant pairwise comparisons (p<0.05), and results are shown as mean
265 ± SEM. **(E)** Similar to (D), except showing the effect of decreasing the electrochemical gradient
266 supporting chloride efflux by increasing extracellular chloride.
267

268 ***A new hypothesis for lateral line mechanotransduction***

269 The MET channels in hair cells are permeable to both monovalent (K^+, Na^+) and divalent (Ca^{2+})
270 cations[7,8]. It has long been speculated that mechanotransduction in lateral line hair cells was
271 mediated by cation influx through the apical membrane, similar to the inner ear. Here we present
272 a new hypothesis: deflection of the hair cell bundle opens MET channels allowing influx of trace
273 amounts of Ca^{2+}, which interacts with Ca^{2+}-activated Cl^- channels, leading to Cl^- efflux through
274 the apical membrane that induces membrane depolarization (Fig. 4). Several lines of evidence
275 support this hypothesis, including 1) the electrochemical gradient across the apical membrane is
276 unable to support cation influx induced depolarization, 2) hair cells only require micromolar
277 extracellular Ca^{2+} to function, 3) the hair cells express Ca^{2+}-activated Cl^- channels, 4) activating
278 these channels induces hair cell depolarization, and 5) blocking these channels reduces the
279 response of animals to mechanosensory stimuli.
280

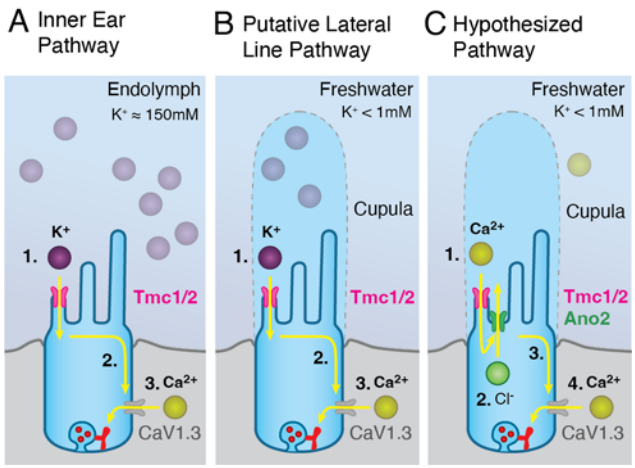

Fig. 4. **Calcium-activated chloride channels amplify hair cell signaling in environments of low ionic strength. (A)** *Established inner ear pathway:* Inner ear hair cells are bathed in a K^+ rich endolymph. 1. As the stereocilia deflect, mechano-electrical transduction (MET) channels open, allowing K^+ influx into the hair cells. 2. Cation influx initiates membrane depolarization. 3. Voltage-gated calcium channels allow Ca^{2+} influx at the basolateral membrane and subsequent vesicle fusion. **(B)** *Putative Lateral Line pathway:* Similar to (A), except the cupula encapsulating the lateral line hair cells maintains an ionic microenvironment that supports K^+ influx. (**C**) *Hypothesized Pathway*: The apical membrane of the lateral line hair cells in zebrafish is exposed to external freshwater environments with insufficient cations to directly drive depolarization. We hypothesize that depolarization is mediated by anion efflux through the following processes: 1. Trace amounts of Ca^{2+} influx through MET channels. 2. Calcium-activated chloride channels open. 3. Cl^- efflux initiates membrane depolarization. 4. Voltage-gated calcium channels support vesicle fusion.

Discussion

Anion efflux mediated sensory transduction provides several potential advantages for cells exposed to ion-poor environments[28]. Anion efflux is expected to be robust to fluctuating external conditions, since the intracellular environment provides a well-regulated source of anions[51] and there is a strong electrochemical gradient supporting efflux across a wide range of external conditions. This intrinsic robustness could allow animals to maintain sensitivity in dynamic environments, without the need for secondary pathways for modulation or auxiliary structures that maintain a stable extracellular microenvironment. Although transduction mechanisms leveraging anion efflux have received much less attention than pathways utilizing cation influx, signal amplification through anion efflux is also found in vertebrate olfactory receptor neurons[22–26]. There, odorant receptors act via a G-protein coupled cascade to increase cAMP, which induces opening of a cyclic-nucleotide-gated cation channel. This leads to an influx of Ca^{2+} and subsequent opening of Ca^{2+}-activated Cl^- channels (Ano2). This striking similarity between mechanoreceptive and olfactory systems, two seemingly disparate sensory modalities, may suggest convergent evolution in systems exposed to dynamic extracorporeal environments.

The lateral line appears to have evolved in early vertebrates[12], but it is not clear if these early vertebrates occupied marine or freshwater environments, or both at different life stages[52,53]. In a marine environment, high Na^+ and Cl^- concentrations at the apical surface would easily support cation influx mediated depolarization and make Cl^- conductance hyperpolarizing. Here, we show that in freshwater environments transduction would require either the establishment of an ionic microenvironment that can support cation influx or a mechanism based on anion efflux. Understanding the evolutionary origins of lateral line hair cells and how these systems evolved as fishes entered new environments would provide important insights into hair cell physiology and the evolution of sensory systems.

The lateral line system continues to serve as a powerful model for dissecting the basic principles of hearing and balance. However, prior studies by our lab and others have typically examined lateral line physiology in ion-rich extracellular saline that mimics vertebrate blood rather than the ion-poor saline these animals naturally inhabit[54,55]. The use of cation-rich saline would be expected to introduce an artificial cation influx while masking naturally occurring anion efflux. As such, this work highlights the necessity of studying sensory systems in the context in which they evolved in order to decipher their true properties and capacities.

References

1. Fettiplace, R. Hair cell transduction, tuning, and synaptic transmission in the mammalian cochlea. *Comprehensive Physiology* **7**, 1197–1227 (2011).
2. Bosher, S. K. & Warren, R. L. Very low calcium content of cochlear endolymph, an extracellular fluid. *Nature* **273**, 377–378 (1978).
3. Smith, C. A., Lowry, O. H. & Wu, M.-L. The electrolytes of the labyrinthine fluids. *The Laryngoscope* **64**, 141–153 (1954).
4. Pan, B. *et al.* TMC1 and TMC2 Are Components of the Mechanotransduction Channel in Hair Cells of the Mammalian Inner Ear. *Neuron* **79**, 504–515 (2013).
5. Pan, B. *et al.* TMC1 Forms the Pore of Mechanosensory Transduction Channels in Vertebrate Inner Ear Hair Cells. *Neuron* **99**, 736-753.e6 (2018).
6. Jia, Y. *et al.* TMC1 and TMC2 Proteins Are Pore-Forming Subunits of Mechanosensitive Ion Channels. *Neuron* **105**, 310-321.e3 (2020).
7. Corey, D. P. & Hudspeth, A. J. Ionic basis of the receptor potential in a vertebrate hair cell. *Nature* **281**, 675–677 (1979).
8. Ohmori, H. Mechano-electrical transduction currents in isolated vestibular hair cells of the chick. *The Journal of Physiology* **359**, 189–217 (1985).

9. Dixon, M. J. *et al.* Mutation of the Na-K-Cl co-transporter gene Slc12a2 results in deafness in mice. *Human molecular genetics* **8**, 1579–1584 (1999).
10. Marcus, D. C., Wu, T., Wangemann, P. & Kofuji, P. KCNJ10 (Kir4. 1) potassium channel knockout abolishes endocochlear potential. *American Journal of Physiology-Cell Physiology* **282**, C403–C407 (2002).
11. Wangemann, P., Liu, J. & Marcus, D. C. Ion transport mechanisms responsible for K+ secretion and the transepithelial voltage across marginal cells of stria vascularis in vitro. *Hearing research* **84**, 19–29 (1995).
12. Jørgensen, J. M. Evolution of the octavolateralis sensory cells. in *The mechanosensory lateral line* 115–145 (Springer, 1989).
13. McHenry, M. J., Feitl, K. E., Strother, J. A. & Van Trump, W. J. Larval zebrafish rapidly sense the water flow of a predator's strike. *Biol. Lett.* **5**, 477–479 (2009).
14. Mekdara, P. J., Schwalbe, M. A. B., Coughlin, L. L. & Tytell, E. D. The effects of lateral line ablation and regeneration in schooling giant danios. *J. Exp. Biol.* **221**, (2018).
15. Olszewski, J., Haehnel, M., Taguchi, M. & Liao, J. C. Zebrafish larvae exhibit rheotaxis and can escape a continuous suction source using their lateral line. *PLoS ONE* **7**, e36661 (2012).
16. Suli, A., Watson, G. M., Rubel, E. W. & Raible, D. W. Rheotaxis in larval zebrafish is mediated by lateral line mechanosensory hair cells. *PLoS ONE* **7**, e29727 (2012).
17. McGlone, F. P., Russell, I. J. & Sand, O. Measurement of calcium ion concentrations in the lateral line cupulae of Xenopus laevis. *Journal of Experimental Biology* **83**, 123–130 (1979).
18. Russell, I. J. & Sellick, P. M. Measurement of potassium and chloride ion concentrations in the cupulae of the lateral lines of Xenopus laevis. *The Journal of physiology* **257**, 245–255 (1976).
19. Nicolson, T. *et al.* Genetic analysis of vertebrate sensory hair cell mechanosensation: the zebrafish circler mutants. *Neuron* **20**, 271–283 (1998).
20. Ricci, A. J. *et al.* Patch-clamp recordings from lateral line neuromast hair cells of the living zebrafish. *Journal of Neuroscience* **33**, 3131–3134 (2013).
21. Zhang, Q. *et al.* Synaptically silent sensory hair cells in zebrafish are recruited after damage. *Nature communications* **9**, 1–16 (2018).
22. Stephan, A. B. *et al.* ANO2 is the cilial calcium-activated chloride channel that may mediate olfactory amplification. *Proceedings of the National Academy of Sciences* **106**, 11776–11781 (2009).

23. Kleene, S. J. & Gesteland, R. C. Calcium-activated chloride conductance in frog olfactory cilia. *J Neurosci* **11**, 3624–3629 (1991).

24. Lowe, G. & Gold, G. H. Nonlinear amplification by calcium-dependent chloride channels in olfactory receptor cells. *Nature* **366**, 283–286 (1993).

25. Cherkashin, A. P. *et al.* Expression of calcium-activated chloride channels Ano1 and Ano2 in mouse taste cells. *Pflugers Arch - Eur J Physiol* **468**, 305–319 (2016).

26. Reisert, J., Lai, J., Yau, K.-W. & Bradley, J. Mechanism of the excitatory Cl- response in mouse olfactory receptor neurons. *Neuron* **45**, 553–561 (2005).

27. Kurahashi, T. & Yau, K.-W. Olfactory Transduction: Tale of an unusual chloride current. *Current Biology* **4**, 256–258 (1994).

28. Reisert, J. & Reingruber, J. Ca2+-activated Cl- current ensures robust and reliable signal amplification in vertebrate olfactory receptor neurons. *Proceedings of the National Academy of Sciences* **116**, 1053–1058 (2019).

29. Spence, R., Gerlach, G., Lawrence, C. & Smith, C. The behaviour and ecology of the zebrafish, Danio rerio. *Biological reviews* **83**, 13–34 (2008).

30. Spence, R. *et al.* The distribution and habitat preferences of the zebrafish in Bangladesh. *Journal of fish biology* **69**, 1435–1448 (2006).

31. Sarin, M. M. & Krishnaswami, S. Major ion chemistry of the Ganga–Brahmaputra river systems, India. *Nature* **312**, 538–541 (1984).

32. Brandt, A., Khimich, D. & Moser, T. Few CaV1.3 Channels Regulate the Exocytosis of a Synaptic Vesicle at the Hair Cell Ribbon Synapse. *J Neurosci* **25**, 11577–11585 (2005).

33. Dezfuli, B. S., Magosso, S., Simoni, E., Hills, K. & Berti, R. Ultrastructure and distribution of superficial neuromasts of blind cavefish, Phreatichthys andruzzii, juveniles. *Microscopy Research and Technique* **72**, 665–671 (2009).

34. Flock, Å. & Jørgensen, J. M. The ultrastructure of lateral line sense organs in the juvenile salamander Ambystoma mexicanum. *Cell and Tissue Research* **152**, 283–292 (1974).

35. Hodgkin, A. L. & Huxley, A. F. A quantitative description of membrane current and its application to conduction and excitation in nerve. *J Physiol* **117**, 500–544 (1952).

36. Beurg, M., Nam, J.-H., Crawford, A. & Fettiplace, R. The actions of calcium on hair bundle mechanics in mammalian cochlear hair cells. *Biophysical journal* **94**, 2639–2653 (2008).

37. Olt, J., Johnson, S. L. & Marcotti, W. In vivo and in vitro biophysical properties of hair cells from the lateral line and inner ear of developing and adult zebrafish. *The Journal of Physiology* **592**, 2041–2058 (2014).

38. Peloggia, J. *et al.* Adaptive cell invasion maintains lateral line organ homeostasis in response to environmental changes. *Developmental Cell* **56**, 1296–1312 (2021).

39. Sand, O. Effects of different ionic environments on the mechano-sensitivity of lateral line organs in the mudpuppy. *Journal of comparative physiology* **102**, 27–42 (1975).

40. Coffin, A. B., Reinhart, K. E., Owens, K. N., Raible, D. W. & Rubel, E. W. Extracellular divalent cations modulate aminoglycoside-induced hair cell death in the zebrafish lateral line. *Hearing research* **253**, 42–51 (2009).

41. Beurg, M., Evans, M. G., Hackney, C. M. & Fettiplace, R. A Large-Conductance Calcium-Selective Mechanotransducer Channel in Mammalian Cochlear Hair Cells. *J. Neurosci.* **26**, 10992–11000 (2006).

42. Di Donato, V., Auer, T. O., Duroure, K. & Del Bene, F. Characterization of the Calcium Binding Protein Family in Zebrafish. *PLoS ONE* **8**, e53299 (2013).

43. Ricci, A. J., Crawford, A. C. & Fettiplace, R. Tonotopic Variation in the Conductance of the Hair Cell Mechanotransducer Channel. *Neuron* **40**, 983–990 (2003).

44. McHenry, M. J., Strother, J. A. & Van Netten, S. M. Mechanical filtering by the boundary layer and fluid–structure interaction in the superficial neuromast of the fish lateral line system. *Journal of Comparative Physiology A* **194**, 795 (2008).

45. Karlsen, H. E. & Sand, O. Selective and Reversible Blocking of the Lateral Line in Freshwater Fish. *Journal of Experimental Biology* **133**, 249–262 (1987).

46. Lush, M. E. *et al.* scRNA-Seq reveals distinct stem cell populations that drive hair cell regeneration after loss of Fgf and Notch signaling. *Elife* **8**, e44431 (2019).

47. Rasche, S. *et al.* Tmem16b is specifically expressed in the cilia of olfactory sensory neurons. *Chem Senses* **35**, 239–245 (2010).

48. deCarvalho, T. N. *et al.* Neurotransmitter map of the asymmetric dorsal habenular nuclei of zebrafish. *Genesis* **52**, 636–655 (2014).

49. Namkung, W., Yao, Z., Finkbeiner, W. E. & Verkman, A. S. Small-molecule activators of TMEM16A, a calcium-activated chloride channel, stimulate epithelial chloride secretion and intestinal contraction. *The FASEB Journal* **25**, 4048–4062 (2011).

50. Pifferi, S., Dibattista, M. & Menini, A. TMEM16B induces chloride currents activated by calcium in mammalian cells. *Pflügers Archiv-European Journal of Physiology* **458**, 1023–1038 (2009).

51. Kaila, K., Price, T. J., Payne, J. A., Puskarjov, M. & Voipio, J. Cation-chloride cotransporters in neuronal development, plasticity and disease. *Nat Rev Neurosci* **15**, 637–654 (2014).

52. Griffith, R. W. Freshwater or marine origin of the vertebrates? *Comparative Biochemistry and Physiology Part A: Physiology* **87**, 523–531 (1987).

53. Halstead, L. B., Chaloner, W. G. & Lawson, J. D. The vertebrate invasion of fresh water. *Philosophical Transactions of the Royal Society of London. B, Biological Sciences* **309**, 243–258 (1985).

54. Olt, J., Johnson, S. L. & Marcotti, W. In vivo and in vitro biophysical properties of hair cells from the lateral line and inner ear of developing and adult zebrafish. *The Journal of Physiology* **592**, 2041–2058 (2014).

55. Lunsford, E. T., Skandalis, D. A. & Liao, J. C. Efferent modulation of spontaneous lateral line activity during and after zebrafish motor commands. *Journal of Neurophysiology* **122**, 2438–2448 (2019).

Methods

Animals

Experiments were performed on 4-7 day post fertilization (dpf) zebrafish larvae (*Danio rerio*), which were raised in bicarbonate-buffered E3 media (5 mM NaCl, 0.17 mM KCl, 0.33 mM $CaCl_2$, 0.33 mM $MgSO_4$, 0.35 $NaHCO_3$, 0.27 µM methylene blue, pH 7.2-7.4; modified from [1]) under standard conditions (28^{o}C, 14:10 light:dark) and provided micropowder feed starting at 5 dpf (Microgemma 75, Skretting). All protocols were approved by the University of Florida Institutional Animal Care and Use Committee.

Cupula ionic composition experiments

Larvae were immobilized by immersion in a paralytic that specifically blocks nicotinic acetylcholine receptors present at the neuromuscular junction (20µL of 1 mg/mL α-bungarotoxin [Sigma Aldrich] in HEPES-buffered E3 [5 mM NaCl, 0.17 mM KCl, 0.33 mM $CaCl_2$, 0.33 mM $MgSO_4$, 1 mM HEPES, titrated to pH 7.2-7.4])[2]. Larvae were transferred to a coverslip-bottomed recording dish at room temperature (20-22°C), pinned onto a small silicone elastomer pad (5 mm x 1 mm x 1 mm, Sylgard 184) using etched tungsten pins (<50 µm diameter) through the notochord, and then this pad was turned over and pinned to a larger block of silicone elastomer such that the lateral side of the animal faced downward. This lateral-side down configuration enabled imaging of the cupula cross-section for predominantly trunk neuromasts on an inverted confocal microscope. Blood flow was taken as a measure of animal health and only trials with robust blood flow at the beginning and end of the experiment were analyzed. The K^+ concentration within the cupula was measured by perfusing on media containing the potassium-selective fluorescent indicator (10 µM IPG-4 in HEPES-buffered E3; ION Biosciences), and recording the fluorescence in the cupula and the surrounding media near the stereocilia (Leica TCS SP5 II, HCX PL APO CS 63x/1.2 water objective, 1 frame/sec, excitation: 514 nm, emission: 530 - 574 nm). Measurements were also made 5 µm and 10 µm above the stereocilia and yielded similar results. Fluorescence values were averaged over a manually selected region-of-interest in ImageJ (v1.48; U. S. National Institutes of Health).

The recorded indicator fluorescence inside of the cupula was not substantially different from the low indicator fluorescence present in the surrounding media, suggesting that the K^+ concentration in the cupula was similar to that of the surrounding media. To ensure that this was not a result of low indicator penetration into the cupula or other issues with fluorescence detection, the relationship between K^+ concentration and indicator fluorescence was then measured *in situ*. The K^+ concentration of the media was incrementally increased by washing in

media with increased KCl (0.2-60 mM total conc.), and changes in the fluorescence within the surrounding media and cupula were recorded. Again, indicator fluorescence inside of the cupula increased in parallel with the surrounding media, suggesting that both the indicator and K^+ penetrate into the cupula. To precisely determine the absolute concentration of K^+ within the cupula under normal conditions (E3 media), these curves were then analyzed using chemical kinetics models. Specifically, fluorescence within the external media was then fit to the Hill equation,

$$\frac{\Delta F}{F_{max}} = \frac{[I]^n}{(K_A)^n + [I]^n} + B_o$$

where ΔF is the fluorescence of the indicator minus the background fluorescence without the indicator, F_{max} is the saturated fluorescence of the indicator minus the background fluorescence, B_o represents the baseline fluorescence of the indicator, K_A is the indicator binding affinity, n is the indicator Hill coefficient, [I] is the K^+ concentration of the media. Fitting was performed using non-linear least squares optimization (Mathworks, MATLAB 2019b). The computed binding constants for IPG-4 were consistent with previously reported values (K_A= 5.7 ± 1.5 mM, mean ± S.E.M.[3]). The K^+ concentration within the cupular matrix under normal conditions (E3 media) was then calculated as

$$[I]_c = \sqrt[n]{\frac{(\Delta F/F_{max} - B_o)\, K_A}{1 - \Delta F/F_{max} + B_o}}$$

where $\Delta F/F_{max}$ is the fluorescence within the cupular matrix as measured in E3 media, normalized by the fluorescence in the cupular matrix at indicator saturation. It should be noted that in this approach the fluorescence values with elevated K^+ media are used only to calibrate the concentration dependence of the indicator molecule (K_A, B_o) and compute the amount of

indicator within the cupula (represented by F_{max}). Any potential effects of elevated K^+ on the physiology of the neuromast would not be expected to modify these results, provided that these effects do not alter the chemical partitioning of the ion indicator between the media and cupular matrix. The difference between the K+ concentration in the cupula and the surrounding media was then compared to zero using a two-tailed one-sample t-test.

The Na^+ concentration was measured using a similar protocol with a different probe (10 µM ING-2 [Ion Biosciences] in HEPES-buffered E3, 5-95 NaCl for calibration, K_A=21.4 ± 3.1 mM[4], excitation: 488 nm, emission: 500-550 nm). To record the Ca^{2+} concentration, animals were first imaged in media containing a Ca^{2+} selective indicator (10 µM Fluo5N [Invitrogen] in HEPES-buffered E3, Ka = 13.4 ± 2.3 µM[5], excitation: 488 nm, emission: 500-550 nm), then the media was replaced by saline solutions with varied Ca^{2+} concentrations (0-2 mM, prepared by varying $CaCl_2$, random order). The difference between the Ca^{2+} concentration in the cupula and media was computed for 20 µM Ca^{2+} media rather than E3 media, since this provides a lower baseline and would be more sensitive to deviations. Similarly, to record the H^+ concentration, animals were imaged in neutral-pH media with a selective probe (10 µM BCECF [Cayman Chemicals] in HEPES-buffered E3 [pH = 7.2], excitation: 496 nm, emission: 477-545 nm), then the media was replaced by saline solutions with varied pH values (first increased to pH=8.4, then decreased to 4.0, prepared by titrating with NaOH or HCl, 5mM MES added to media for solutions with pH < 6.8). Since BCECF is quenched, this calibration curve was fit to the Stern-Volmer equation instead of the Hill equation and F_{max} was taken as the fluorescence at the highest examined pH value, but calculations were otherwise similar. The Cl^- concentration within the cupular matrix was measured using the fluorescent indicator MQAE (1 mM in HEPES-buffered E3). In order to provide excitation at the short UV wavelengths required by MQAE, imaging was performed using two-photon microscopy (custom-built system, Zeiss

20x/1.0 objective, Coherent Chameleon Vision II laser, 750 nm excitation, Chroma HQ480/40M emission filter). Since the MQAE could be visualized quickly penetrating through the cupula and to limit the potential for UV-induced damage, the indicator calibration was performed in a separate series of experiments without the animal (0-50mM KCl) rather than with the animal as above. To produce a calibration curve, the fluorescence at each Cl^- concentration was normalized by the fluorescence recorded for saline with a Cl^- concentration equal to E3 media. The fluorescence measured in the cupula was then normalized by the fluorescence in the surrounding media, and this value was compared to the calibration curve to calculate the concentration of Cl^- in the cupula.

Membrane reversal potentials

The membrane reversal potentials for the MET channel of the lateral line hair cells in different extracellular salines were estimated using a modified constant field equation that includes the contributions of Ca^{2+} (modified GHK equation[6,7]). The examined extracellular concentrations were centered around the values for E3 media, and the intracellular ionic composition was assumed to be similar to other neurons ($[Na^+]_{out}$ = 5 mM, $[Na^+]_{in}$ = 5 mM, $[K^+]_{out}$ = 0.17 mM, $[K^+]_{in}$ = 130 mM, $[Ca^{2+}]_{out}$ = 0.33 mM, $[Ca^{2+}]_{in}$ = 100 nM, 28°C, [8]). The relative permeabilities of MET channels were estimated based on measurements from hair cells in other species: $P(Ca^{2+})$ = 5, P(K+) = 1.15, $P(Na^+)$ = 1,[9–11]. For comparison, the reversal potential for selective chloride conductance was also estimated using the Nernst equation ($[Cl^-]_{in}$ = 10 mM, 28°C,[12]). The calculated reversal potentials were compared against the opening potential for the voltage-gated Ca^{2+} channels on the basolateral membrane (CaV1.3, estimated at -50mV,[13–16]).

Cupula diffusion experiments

Animals were prepared as in the cupula ionic composition experiments. We visualized the precise boundary of the cupula by immersing the animals in fluorescent polystyrene microspheres and allowing them to coat the cupula (200 nm, suncoast yellow, FSSY002, Bang Labs; 1:100 in HEPES-buffered E3, [17]). The permeability of the cupular matrix was measured by recording the penetration of a negatively-charged fluorophore (6-carboxyfluorescein; Sigma-Aldrich) into the cupula. The fluorophore (10 μM in HEPES-buffered E3) was loaded into a glass pipette (tip diameter: ~5 μm; Model P-97 Flaming/Brown Micropipette Puller, Sutter Instrument Co.) aimed ~20 μm away at the cupula. The pipette pressure was then rapidly increased by opening a valve attached to a pressure source (100 torr, Fluke Biomedical Instruments DPM1B), dye surrounded the cupula, and the change in fluorescence over time was recorded at the stereocilia level (Leica TCS SP5, HCX PL APO CS 63x/1.2 water objective, 20 frames/sec, excitation: 488 nm; emission: 500 - 550 nm). Values for $\Delta F/F_{max}$ were computed by subtracting the fluorescence prior to dye release, and then normalizing by the maximum fluorescence following release. The time constant for the increase in dye fluorescence was fit to an exponential waveform

$$\frac{\Delta F}{F_{max}} = 1 - e^{-t/\tau}$$

where F_{max} is the maximum fluorescence, τ is the time constant, and t is time. Fitting was performed using non-linear least-squares fitting (Mathworks, MATLAB R2020b). Relative time constants were calculated as the ratio of the time constant in the cupula divided by the time constant in the surrounding media for the same trial. Differences were identified by comparing this relative time constant to one using a two-tailed one-sample t-test.

Computational cupula diffusion model

Simulations of the fluorophore diffusion experiments were performed by modeling the cupula as a cylinder (13 µm diameter, 40 µm height, [17]) of uniform material with an isotropic diffusion coefficient. Since the pipette jet rapidly replaced the fluorophore solution at the periphery of the cupular during experiments, the fluorophore concentration was assumed to be uniform over the exposed surface of the cupula and increase following an exponential waveform with parameters estimated from the imaging data, see cupula diffusion experiments). Diffusion is a linear process and the absolute fluorophore concentration does not alter the dynamics, so the concentration was arbitrarily selected to ramp from zero to one. The cylinder was discretized using an all-tetrahedral mesh and Fick's equation was solved for this geometry using a commercial finite element method solver (Comsol 6.0). A sensitivity analysis was performed to ensure that mesh density and time stepping were adequate. Although the central problem is axisymmetric, a 3-dimensional mesh was used as some sensitivity analyses included non-axisymmetric convective terms. This model was then solved for a logarithmic series of cupular matrix diffusion coefficients surrounding the value recorded for the fluorophore in free water ($1x10^{-12}$ to $1x10^{-9}$ m^2/s, $D_{6CF} = 0.487x10^{-9}$, [18]), and the predicted temporal profile of the fluorophore at the center of the cupula was calculated for each condition. The cupular diffusion coefficient was then estimated by comparing the time constants from these simulations to the time constants obtained from the imaging experiments.

Computational Nernst-Planck model

We performed a series of computational studies to determine how K^+ secretion at the apical surface of the neuromast would affect K^+ concentrations within the cupula. The cupula was modeled as a cylinder (13 µm diameter, 40 µm height, [17]) immersed in an infinitely large electrolyte bath (spherical bubble with radius of 100 µm explicitly modeled, surrounding volume

592 modeled using infinite element domain). The ion currents and concentrations within the cupula
593 and surrounding media were modeled using the full Nernst-Planck equations subject to the
594 electroneutrality approximation and solved using a commercial finite element method
595 multiphysics package (Comsol 6.0). In addition to water, the electrolyte included K^+, Na^+, and
596 Cl^- ions and the self-diffusion coefficients for each ion in the surrounding media were taken from
597 previously reported values (K^+: $1.89x10^{-9}$, Na^+: $1.33x10^{-9}$, Cl^-: $2.06x10^{-9}$ m^2/s, [19,20]). The model
598 was solved for two configurations: the most probable scenario in which the ion diffusion
599 coefficients in the cupular matrix are equivalent to those in water, and a conservative model in
600 which the diffusion coefficient of each ion was scaled down to match the lower bound of the
601 95% CI for the relative diffusion coefficient obtained in the 6-CF experiments (6.9% of free
602 water). The electrical mobility of each species was estimated using the Nernst-Einstein relation.
603 The model was solved using a steady-state axisymmetric system, the cupula and explicit media
604 domain were meshed using free triangular elements, the infinite element domain was meshed
605 with mapped quadrilateral elements, and a sensitivity analysis was used to confirm that the mesh
606 density was sufficient. The boundary conditions were set such that at infinity the electrical
607 potential was zero and the ion concentrations were equal to those of E3 media (0.17 mM K^+, 5
608 mM Na^+, 5.17 mM Cl^-), the surface of the body was impermeable to all ions, and the base of the
609 cupula secreted K^+ ions at a fixed rate. Simulations were performed for a logarithmic series of K^+
610 secretion currents spanning a wide range ($1x10^{-10}$ – $1x10^{-6}$ A), and K^+ concentrations at the base
611 of the cupula and in the surrounding media were computed for each current value. Results were
612 qualitatively similar for the water-like diffusion configuration and the conservative configuration
613 with scaled down diffusion coefficients, although the conservative configuration yielded higher
614 K^+ concentrations within the cupula as expected (reaching a K^+ concentration of 10.2 mM at the

615 apical surface requires 56 nA for a diffusion coefficient equal to water, and 4.8 nA for a
616 diffusion constant at the lower bound of the 95% confidence interval).
617
618 Calcium imaging
619 We examined the responses of the lateral line hair cells to mechanical stimuli in environmental
620 salines with varying ionic compositions. Larvae (5 -7dpf) expressed the membrane-localized
621 fluorescent calcium indicator gCaMP6s-CAAX in hair cells (*myo6b:gCaMP6s-CAAX*, [21]), and
622 were immobilized and imaged as described above (in HEPES-buffered E3). A glass bead (5 µm)
623 attached to a piezoelectric transducer (30V300, Piezosystem Jena) was positioned approximately
624 10 µm anterior from the distal end of the neuromast kinocilia[22,23]. During each trial, a stimulus
625 program (Clampex 10.1) controlled via a low-noise digitizer (Digidata 1440A) elicited three
626 sweeps of sinusoidal movement (5 Hz) for 20 seconds that were preceded and followed by
627 inactivity of equal duration. The glass bead vibrated, deflecting the cupula in the anterior-to-
628 posterior direction. Cupula deflection was monitored by measuring the displacement distance of
629 the kinocilia tips (~10 µm). Mechanosensitive Ca^{2+} responses were measured within the hair
630 cells (Leica TCS SP5 II, HCX PL APO CS 63x/1.2 water objective, 5 frames/sec, excitation:
631 488□nm, emission: 501 - 583 nm). Between trials, the perfusate bath was replaced using media
632 with decreased total Ca^{2+} concentration (20 µM Ca^{2+}: HEPES-buffered E3 with reduced $CaCl_2$,
633 or 0 µM Ca^{2+}: HEPES-buffered E3 with $CaCl_2$ replaced by equivalent concentration of $MgSO_4$).
634 Preliminary experiments performed in media containing EGTA (0.2 mM) yielded similar results
635 to 0 µM Ca^{2+} trials, suggesting these solutions contained negligible residual calcium. Responses
636 to stimuli were quantified by finding the mean fluorescence within manually selected regions of
637 interest (ROI) for individual hair cells (ImageJ). Fluorescence values were then used to compute
638 ΔF/F by subtracting and then normalizing by the baseline fluorescence computed from the mean

fluorescence within the cell prior to stimulation. Responses were detected by comparing the time-average of the ΔF/F during stimulus periods to non-stimulus periods using a paired two-tailed t-test. Changes in response amplitude were identified by comparing the time-average during stimulus periods between treatment groups (20 μM Ca^{2+} and 0 μM Ca^{2+} media) and the control (E3 media) using a paired two-tailed t-test.

A similar protocol was used to examine the responses of hair cells to a calcium-activated chloride channel agonist. Baseline activity was recorded for 30 s in freshwater media (E3 saline), then perfused with Eact (50 μM in 0.1% DMSO final conc., [24]). We monitored changes in fluorescence before, during, and after perfusion of Eact (0.8 frames/sec, excitation: 488 nm, emission: 500 nm - 600 nm). Relative changes in fluorescence were quantified using regions of interest around responsive hair cells. Mean ΔF/F during the 30 sec prior to Eact exposure was then compared to the mean response for 60 sec following Eact exposure using a paired two-tailed t-test.

Behavioral assays

The behavioral response of zebrafish larvae (5-7 dpf, AB strain) to mechanical stimuli was assessed using a custom-developed behavioral assay. This assay was conducted in an enclosure that maintains a constant internal temperature (28°C, using Fisher Scientific IsoTemp 6200 R28) and isolates experiments from ambient light and noise. Animals were transferred into a dish containing the experimental media (38 mm diameter, 6 mm height) to incubate (20 min for all trials except neomycin, which incubated for 1 h), then transferred into the behavioral chamber and allowed to acclimate briefly (5 min) prior to experiments. The behavioral chamber was designed to operate as an oscillatory Couette cell, which produces shear stress in the fluid but not pressure waves [25]. This chamber was laser cut from acrylic sheet and provided a cylindrical

raceway (35 mm outer diameter, 25 mm inner diameter, filled to depth of 5 mm) that was suspended by flexible struts. These flexible struts functioned as a flexure bearing system, allowing oscillatory rotations of the raceway about the cylindrical axis while preventing translation or other rotations. Oscillatory rotations were driven using a fourth, rigid strut that was affixed with adhesive to the center dome of a speaker (Soberton SP-3114Y), which was connected to an audio amplifier (Adafruit 987, MAX98306). The chamber was diffusely illuminated from above with white light (ST-WP-5050-DL-RL, TheLEDLight.com) to maintain normal swimming behavior.

Stimulus generation was controlled via a custom-written MATLAB script (Mathworks, R2020b) and a data acquisition system (National Instruments, PCIe-6323). Each experiment consisted of a baseline activity recording period (300 s) followed by a series of 35 trials with stimuli. Each trial began with a 2 s mechanical stimulus (20 Hz, 5 amplitudes with 7 replicates each, randomly ordered) followed by a randomized interstimulus interval (mean: 120 s, std. dev.: 20 s, min: 60 s, max: 180 s). The magnitude of the stimulus was calibrated by imaging the rigid strut of the raceway using a high-speed camera system (Phantom Miro 340, 200 fps, Samyang 1.4/85mm lens, 68 mm of extension tubes) and computing the displacement with sub-pixel precision using a custom-written MATLAB script. Reported stimulus amplitudes represent the displacement amplitude at the outer wall of the raceway.

The movement of the animals was continuously recorded and used to assess the response to the mechanical stimulus. A sheet of rear screen projection material (GooScreen BlackMax 1950) was positioned beneath the behavioral arena and illuminated with near-infrared light (850nm, ThorLabs 850L3). Animals were then imaged using a NIR-sensitive camera positioned above the arena (30 frames/sec, Point Grey GS3-U3-41C6NIR) equipped with a NIR-transmissive lens (Schneider 50mm Xenoplan, 1001976) and visible light blocking filter (Lee

Filter #87). During each stimulus period, a small NIR LED positioned within the field of view was automatically illuminated, and this light was used to synchronize the stimuli with the recorded video to within one frame. The position of the larvae in each image frame was calculated using previously developed MATLAB scripts (https://bitbucket.org/jastrother/larval_proving_grounds).

The response to each stimulus was scored based on the induced change in the swimming speed of the larvae. In order to quantify each response in a way that was independent of the average swimming speed of the animal, each trial was scored as a response if the stimulus elicited a change in the swimming speed that fell outside of the 95% confidence interval computed for similar stimulus-free periods. Specifically, the average swimming speed of the animals was computed for 3 time windows: a first reference window (500 ms duration, ending 10 s prior to the stimulus), a second reference window (500 ms duration, ending 5 s prior to the stimulus), and a response window (500 ms duration, starting with the stimulus). The difference between the first and second reference window was aggregated and used to compute the cumulative probability distribution of the spontaneous swimming speed change during a stimulus-free period for each individual. The difference between the second reference window and the response window was compared to this distribution, and each trial was marked as a response if it fell below the 2.5% percentile or above the 97.5% percentile. Since this approach yields an expected false positive rate of 5%, the calculated response probabilities were offset by the same amount.

Differences in the response probability between experimental and control groups were detected with two different statistical analyses. First, multinomial probit regression was used to implement an omnibus test that detects differences between the experimental and control groups while integrating information across stimulus intensities (Mathworks, MATLAB R2020b).

Second, pairwise differences between the experimental and control groups at specific stimulus intensities were detected using Fisher's exact test with false discovery rate control implemented using the Benjamini-Hochberg procedure (Mathworks, MATLAB R2020b). Plots include error bars representing S.E.M. values, where the variance was calculated using the properties of binomial distribution [p (1-p)].

The following conditions were examined: "HEPES-buffered E3 media" (5 mM NaCl, 0.17 mM KCl, 0.33 mM $CaCl_2$, 0.33 mM $MgSO_4$, 1 mM HEPES, titrated to pH 7.2-7.4 with HCl/NaOH), "200 µM Neomycin media" (200 µM neomycin sulfate in HEPES-buffered E3 media), "50 µM niflumic acid" (50 µM niflumic acid in HEPES-buffered E3 media with 0.05% DMSO), "3x Ionic Strength media" (NaCl and KCl increased 3x relative to E3: 15 mM NaCl, 0.51 mM KCl, 0.33 mM $CaCl_2$, 0.33 mM $MgSO_4$, 1 mM HEPES, titrated to pH 7.2-7.4 with HCl/NaOH), "20x Ionic Strength media" (NaCl and KCl increased 20x relative to E3: 100 mM NaCl, 3.4 mM KCl, 0.33 mM $CaCl_2$, 0.33 mM $MgSO_4$, 1mM HEPES, titrated to pH 7.2-7.4 with HCl/NaOH), "0.8 mM Cl^- media" (replace NaCl with Na-Gluconate in E3: 5 mM Na-Gluconate, 0.17 mM KCl, 0.33 mM $CaCl_2$, 0.33 $MgSO_4$, 1 mM HEPES, titrate to pH 7.2-7.4 with citric acid/NaOH), "16 mM Cl^- media" (major cations matched to E3, approximately isosmotic to 3x Ionic Strength media: 5mM NaCl, 10.3 mM NMDG-Cl, 0.17 mM KCl, 0.33 mM $CaCl_2$, 0.33 $MgSO_4$, 1mM HEPES, pH 7.2-7.4), "104 mM Cl^- media" (major cations matched to E3, approximately isosmotic to 20x Ionic Strength media: 5 mM NaCl, 98.22 mM NMDG-Cl, 0.17 mM KCl, 0.33 mM $CaCl_2$, 0.33 mM $MgSO_4$, 1mM HEPES, titrated to pH 7.2-7.4 with HCl/NaOH), and "20 µM Ca^{2+} media" (replace Ca^{2+} with Mg^{2+} in E3: 5 mM NaCl, 0.17 mM KCl, 20 µM $CaCl_2$, 0.31 mM $MgCl_2$, 0.33 mM $MgSO_4$, 1 mM HEPES, titrated to pH 7.2-7.4 with HCl/NaOH). The HEPES-buffered E3 media served as the control for all experimental groups, and control trials were run in parallel with experimental trials. Since the responses from

735 control trials exhibited very little inter-clutch variation, data from control trials was pooled when
736 performing statistical analyses. At least 3 clutches of embryos were used for all conditions, and
737 parents were randomly selected from a genetically diverse population.
738
739 Analysis of transcriptomic data
740 In order to identify gene products that may be contributing to the mechanotransduction process,
741 we conducted a survey of previously published lateral line neuromast scRNA-seq data [26]. A
742 MATLAB script (Mathworks, R2020B) was written that performed the following steps: cells
743 that express the hair cell marker *tmc2b* were selected, the transcripts expressed by each selected
744 cell were filtered to include genes annotated with a relevant list of ontology terms ("ion
745 transport", "ion channel activity", "gpcr activity", "chemical synaptic transmission", "hormone
746 activity", "neuropeptide hormone" for *Danio rerio* in AmiGo2[27] and a manually curated listed of
747 similar genes not captured in the gene ontology database (based on searches of zfin.org[28]), and
748 the resulting list was then reviewed to identify genes with known anion efflux activity. This
749 analysis was performed exclusively for hypothesis generation. To avoid issues with
750 pseudoreplication, further examination of the genes of interest was performed in independent
751 experiments (e.g., *in situ* hybridization) rather than a statistical analysis of the same
752 transcriptome dataset.
753
754 *In situ* hybridization
755 The expression of *ano2b* was examined using HCR RNA-FISH[29] following protocol based on
756 the manufacturer's directions. Briefly, larvae (AB strain, 4 dpf) were cold anesthetized and fixed
757 with 4% PFA in PBS (overnight at 4°C), washed with PBS (3x, 5 min, room temperature [RT]),
758 dehydrated with a PBS/MeOH series (75/25%, 50/50%, 25/75%, 0/100%, 5 min each at RT),

759 frozen (1 hr at -20°C), rehydrated with a MeOH/PBST series (75/25%, 50/50%, 25/75%,
760 0/100%, 5 min each at RT, PBST: PBS with 0.1% Tween 20), incubated in hybridization buffer
761 (20 min at 37°C), hybridized with *ano2b* probes (20 nM, overnight at 37°C), washed with probe
762 wash buffer (4x, 15 min, 37°C), washed with 5X SSCT (2x, 5 min, RT; SSCT: SSC with 0.1%
763 Tween 20), incubated in amplification buffer (30 min, RT), incubated with snap-cooled
764 amplifiers in amplification buffer (60 nM each, 18 h, RT), washed with 5X SSCT (2x 5 min, 2x
765 30 min, 1x 5 min, RT), labeled with DAPI (30 min, 1 µM in 5X SSCT, RT), and imaged on a
766 confocal microscope (Leica TCS SP5, HCX PL APO CS 63x/1.2 water objective for hair cells,
767 HC PL Fluotar 20x/0.5 objective for others, DAPI: excitation = 405 nm, emission = 415 - 485
768 nm, AlexaFluor 647: excitation = 633 nm, emission = 695 - 765 nm). Images were collected of
769 superficial neuromasts, olfactory epithelium, and the CNS. Images were also collected from
770 randomly selected regions along the trunk adjacent to superficial neuromasts, in order to verify
771 that the observed labeling of superficial neuromasts was not a product of non-specific surface
772 labeling.
773

774 **Methods References**

775 1. Nusslein-Volhard, C. & Dahm, R. *Zebrafish*. (OUP Oxford, 2002).
776 2. Lunsford, E. T. & Liao, J. C. Activity of Posterior Lateral Line Afferent Neurons during Swimming in
777 Zebrafish. *JoVE (Journal of Visualized Experiments)* e62233 (2021) doi:10.3791/62233.
778 3. Rana, P. S. *et al*. Calibration and characterization of intracellular Asante Potassium Green probes, APG-2 and
779 APG-4. *Anal Biochem* **567**, 8–13 (2019).
780 4. Iamshanova, O., Mariot, P. & Prevarskaya, N. Comparison of fluorescence probes for intracellular sodium
781 imaging in prostate cancer cell lines. *European Biophysics Journal* **45**, 765–777 (2016).
782 5. Kabbara, A. A. & Allen, D. G. The use of the indicator fluo-5N to measure sarcoplasmic reticulum calcium in
783 single muscle fibres of the cane toad. *J Physiol* **534**, 87–97 (2001).

6. Lewis, C. A. Ion-concentration dependence of the reversal potential and the single channel conductance of ion channels at the frog neuromuscular junction. *The Journal of Physiology* **286**, 417–445 (1979).

7. Jan, L. Y. & Jan, Y. N. Properties of the larval neuromuscular junction in Drosophila melanogaster. *The Journal of Physiology* **262**, 189–214 (1976).

8. Olt, J., Johnson, S. L. & Marcotti, W. In vivo and in vitro biophysical properties of hair cells from the lateral line and inner ear of developing and adult zebrafish. *The Journal of Physiology* **592**, 2041–2058 (2014).

9. Pan, B. *et al.* TMC1 and TMC2 Are Components of the Mechanotransduction Channel in Hair Cells of the Mammalian Inner Ear. *Neuron* **79**, 504–515 (2013).

10. Pan, B. *et al.* TMC1 Forms the Pore of Mechanosensory Transduction Channels in Vertebrate Inner Ear Hair Cells. *Neuron* **99**, 736-753.e6 (2018).

11. Lumpkin, E. A., Marquis, R. E. & Hudspeth, A. J. The selectivity of the hair cell's mechanoelectrical-transduction channel promotes Ca^{2+} flux at low Ca^{2+} concentrations. *Proc. Natl. Acad. Sci. U.S.A.* **94**, 10997–11002 (1997).

12. Glykys, J. *et al.* Local impermeant anions establish the neuronal chloride concentration. *Science* **343**, 670–675 (2014).

13. Brandt, A., Khimich, D. & Moser, T. Few CaV1.3 Channels Regulate the Exocytosis of a Synaptic Vesicle at the Hair Cell Ribbon Synapse. *J Neurosci* **25**, 11577–11585 (2005).

14. Platzer, J. *et al.* Congenital deafness and sinoatrial node dysfunction in mice lacking class D L-type Ca2+ channels. *Cell* **102**, 89–97 (2000).

15. Putzier, I., Kullmann, P. H. M., Horn, J. P. & Levitan, E. S. Cav1.3 channel voltage dependence, not Ca2+ selectivity, drives pacemaker activity and amplifies bursts in nigral dopamine neurons. *J Neurosci* **29**, 15414–15419 (2009).

16. Xu, W. & Lipscombe, D. Neuronal Ca(V)1.3alpha(1) L-type channels activate at relatively hyperpolarized membrane potentials and are incompletely inhibited by dihydropyridines. *J Neurosci* **21**, 5944–5951 (2001).

17. Van Trump, W. J. & McHenry, M. J. The morphology and mechanical sensitivity of lateral line receptors in zebrafish larvae (Danio rerio). *Journal of Experimental Biology* **211**, 2105–2115 (2008).

18. Kramer, E. M., Frazer, N. L. & Baskin, T. I. Measurement of diffusion within the cell wall in living roots of Arabidopsis thaliana. *Journal of experimental botany* **58**, 3005–3015 (2007).

19. Hawlicka, E. Self-diffusion of sodium, chloride and iodide ions in acetonitrile-water mixtures. *Zeitschrift für Naturforschung A* **42**, 1014–1016 (1987).
20. Friedman, A. M. & Kennedy, J. W. The self-diffusion coefficients of potassium, cesium, iodide and chloride ions in aqueous solutions1. *Journal of the American Chemical Society* **77**, 4499–4501 (1955).
21. Zhang, Q. *et al.* Synaptically silent sensory hair cells in zebrafish are recruited after damage. *Nature communications* **9**, 1–16 (2018).
22. Haehnel-Taguchi, M., Akanyeti, O. & Liao, J. C. Afferent and motoneuron activity in response to single neuromast stimulation in the posterior lateral line of larval zebrafish. *J Neurophysiol* **112**, 1329–1339 (2014).
23. Skandalis, D. A., Lunsford, E. T. & Liao, J. C. Corollary discharge enables proprioception from lateral line sensory feedback. *PLoS Biol* **19**, e3001420 (2021).
24. Namkung, W., Yao, Z., Finkbeiner, W. E. & Verkman, A. S. Small-molecule activators of TMEM16A, a calcium-activated chloride channel, stimulate epithelial chloride secretion and intestinal contraction. *The FASEB Journal* **25**, 4048–4062 (2011).
25. Lamb, H. *Hydrodynamics*. (Dover, 1945).
26. Lush, M. E. *et al.* scRNA-Seq reveals distinct stem cell populations that drive hair cell regeneration after loss of Fgf and Notch signaling. *Elife* **8**, e44431 (2019).
27. The Gene Ontology resource: enriching a GOld mine. *Nucleic acids research* **49**, D325–D334 (2021).
28. Bradford, Y. M. *et al.* Zebrafish Information Network, the knowledgebase for Danio rerio research. *Genetics* **220**, iyac016 (2022).
29. Choi, H. M. *et al.* Third-generation in situ hybridization chain reaction: multiplexed, quantitative, sensitive, versatile, robust. *Development* **145**, dev165753 (2018).

Acknowledgments: We thank K. Kindt for providing plasmids and transgenic zebrafish embryos, J. Ryan for his insights on transcriptome analysis, and the UF Center for Taste and Smell for its support. Funding provided by: National Science Foundation (IOS1932707 to JAS; IOS1257150, IOS1855956, & IOS1856237 to JCL), Paul G. Allen Frontiers Group (to JAS), and National Institutes of Health (R01DC010809 to JCL).

Author contributions:

ETL, YVB, JCL, and JAS conceived the study and designed the methodology. ETL, YVB, and JAS conducted imaging experiments and analyzed the data. BCR and JAS conducted behavioral experiments and analyzed the data. ETL, YVB, JCL, and JAS interpreted the results. ETL, BCR, JCL, and JAS contributed to the first draft of the manuscript, and all authors contributed to reviewing and editing the manuscript.

Competing interests: Authors declare that they have no competing interests.

Additional Information:

Correspondence and requests for materials should be addressed to James Strother.

Data and materials availability: All data and code used for analysis will be made available upon request.

Extended Data Figures

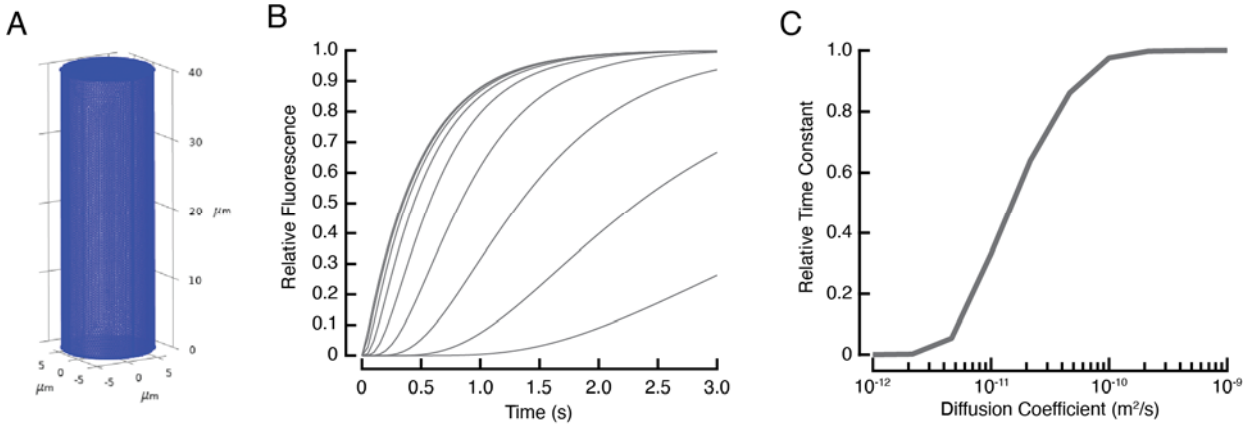

Extended Data Fig. 1: Computational simulations support cupula diffusion experiments. **(A)** Mesh used for finite element modeling. **(B)** Simulated time series for a position just above the base of the cupula (8 μm) for a range of diffusion coefficients ($1x10^{-12}$, $2.15x10^{-12}$, $4.64x10^{-12}$, $1x10^{-11}$, $2.15x10^{-11}$, $4.64x10^{-11}$, $1x10^{-10}$, $2.15x10^{-10}$, $4.64x10^{-10}$, $1x10^{-9}$ m^2/s). **(C)** Simulated relative time constant as a function of the modeled diffusion coefficient. Comparison of experimental and modeling results indicate that the diffusion of the charged fluorophore 6-CF through the cupular matrix is similar to that through water ($D = 0.034x10^{-9} – 0.487x10^{-9}$ m^2/s, 6.9%-100% of water, 95% CI), with the lower bound of the estimate limited by the achievable dye injection speed of the experimental apparatus.

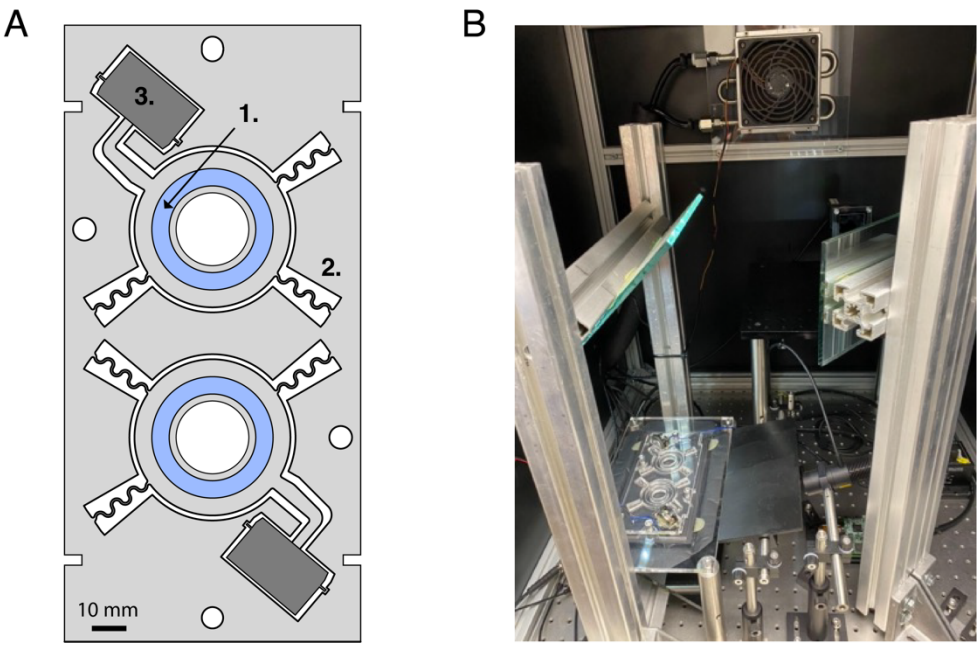

868

869 **Extended Data Fig. 2: Apparatus used for behavioral assays. (A)** Outline of the behavioral

870 arena, showing circular racetrack in which larva swims [1], which is suspended by flexure

871 bearings [2] and driven by a speaker [3]. Each apparatus contains two chambers that are operated

872 in parallel. **(B)** Image of behavioral assay in temperature controlled enclosure.

873

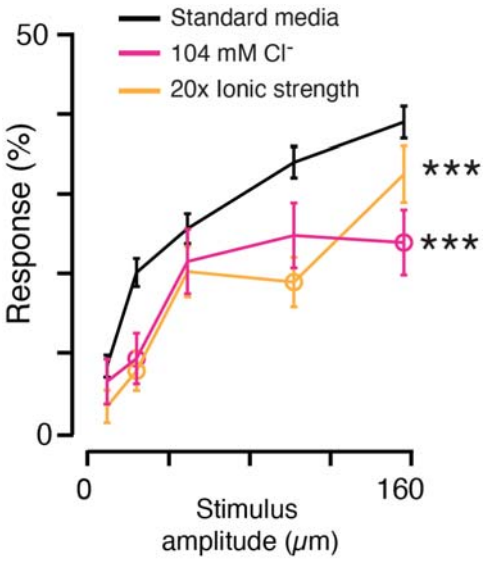

Extended Data Fig. 3: Zebrafish larvae display reduced lateral line sensitivity in environmental saline solutions with higher ionic strength. The response probability of zebrafish larvae to mechanical stimuli of different intensities in various environmental saline solutions, as measured using the oscillatory Couette behavioral assay. Asterisks indicate statistically significant differences integrated across stimulus intensities (*p<0.05, **p<0.01, ***p<0.001), open circles represent significant pairwise comparisons (p<0.05), and results are shown as mean ± SEM.

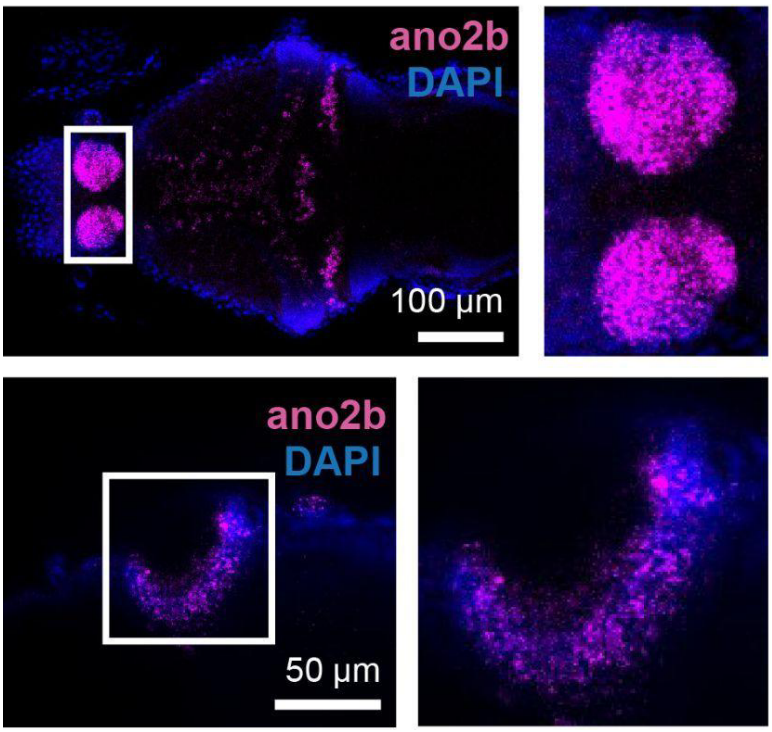

883

884 **Extended Data Fig. 4:** *In situ* hybridization for *ano2* labels the dorsal habenula (top, magnified

885 right) and the olfactory epithelium (bottom, magnified right).

886